Effect of lattice and dopant–induced strain on the conductivity of solid electrolytes: application of the elastic dipole method

Ashkan Moradabadi[a,b], Payam Kaghazchi[c,*]

[a] *Institut für Chemie und Biochemie, Freie Universität Berlin, Takustr. 3, 14195 Berlin, Germany*
[b] *Max Planck Institute for Solid State Research, Heisenbergstr. 1, 70569 Stuttgart, Germany*
[c] *Forschungszentrum Jülich GmbH, Institute of Energy and Climate Research (IEK-1), Materials Synthesis and Processing, 52425 Jülich, Germany*

Abstract

The elastic dipole method (EDM) is applied to predict the response of defect formation and migration energies to an external strain field (ϵ_{ij}) within the elastic regime. EDM provides an analytical expression for the energy variations in a system with a point defect as a function of ϵ_{ij}. Although EDM has so far been employed for various simple semiconductors and insulators, it has not been yet applied for complex solid ionic conductors that are used as solid electrolytes in all-solid-state batteries (ASSBs). In the present study, we have considered two promising Li-based ASSB electrolytes, namely Al-doped cubic $Li_{6.25}Al_{0.25}La_3Zr_2O_{12}$ (Al-LLZO) and $Li_{10}GeP_2S_{12}$ (LGPS) to investigate the impact of elastic strain on Li-defect formation energy and migration barrier by performing a direct method (manually-applied strain) and EDM. It is shown that EDM can quantitatively provide accurate values for Li-defect formation energy as a function of ϵ_{ij}. EDM can also predict, qualitatively, how the migration barrier varies with ϵ_{ij}. In both Al-LLZO and LGPS systems, the formation energy of Li^+ vacancy decreases (increases) by applying a tensile (compressive) strain, which is because the lattice parameters tend to expand by formation of a Li^+ vacancy. An opposite behavior is found for the formation energy of interstitial Li^+. In addition, both the direct method and EDM show that the impact of strain on Li ion migration energy is not similar in

*Corresponding author
Email address: p.kaghazchi@fz-juelich.de (Payam Kaghazchi)

Al-LLZO and LGPS. A compressive strain decreases the barrier in the former case, while it increases it in the latter case. The lowering of migration barrier in Al-LLZO is in spite of contraction of bottleneck width of Li diffusion in this system. A similar finding has also been reported by a recent experimental study. Analysis of EDM results shows that the lowering (rising) in the migration barrier of Li in Al-LLZO (LGPS) under a compressive strain is due to tendency of the system to contract (expand) Li–O (Li–S) bond lengths in the transition states where Li ions are at the bottlenecks of diffusion pathways. We finally show that the result of Li migration barrier as a function of strain in a non-doped solid electrolyte can be used to predict the global effect of substitution/doping (lattice size variation) on the conductivity of that system.

Keywords:

Stress/Strain, Defect Formation, Li ion Migration, Solid Electrolytes, Elastic Dipole Method

---

1. INTRODUCTION

All-solid-state battery (ASSB) is currently an active and critical area of research and development [1, 2]. Despite relatively high thermal and mechanical stability of developed solid electrolytes (SEs), there exist two major problems, namely low ionic conductivity and poor chemical stability, to solve in order to use these materials for ASSBs[1]. There are several strategies to tune the ionic conductivity of battery materials, such as applying strain [3, 4, 5], doping [6, 7], nanosizing [8, 9], and tailoring the microstructure [10, 11]. In fact, the last three procedures lead to creation, suppression, or enhancement of lattice strain. Therefore, understanding the effect of strain on ionic conductivity of SEs is essential. To achieve this goal, it is necessary to find the impact of external strain on both formation and migration of charge carriers.

$Li_{6.25}Al_{0.25}La_3Zr_2O_{12}$ (Al-doped cubic LLZO, hereafter called Al-LLZO) and $Li_{10}GeP_2S_{12}$ (LGPS) are of most widely-studied oxide- and sulfide-based SEs, respectively [1]. Defect chemistry in Al-LLZO has been studied using experimental [12, 13] and theoretical [14, 15] methods. *Ab initio*-based thermodynamics calculations in our previous study [14] confirmed the formation of complex defects of Li^+ and O^{2-} vacancies reported by experimental measurements. However, this theoretical study [14] found that a negatively charged Li vacancy together with a positively charged interstitial Li (Li Frenkel pair) is the dominant type of defect for a wide range of Fermi energy and Li chemical potential values providing the charge neutrality in this system. This result is in line with ionic conductive nature of Al-LLZO. Oh *et al.* [16] have studied the defect chemistry in LGPS using a similar approach to ref. [14] and shown that the Li Frenkel pair is also a favorable defect type under the charge neutrality in bulk LGPS.

Mechanism of Li transport in c-LLZO as well as tetragonal LLZO and LGPS has been extensively explored in many experimental and theoretical studies [17, 18, 19, 20, 21, 22, 23, 24, 25, 26, 27, 28, 29, 30, 31, 32, 33, 34, 35, 36, 37]. Regarding c-LLZO, although a pure concerted mechanism for Li migration has been reported by Jalem *et al.* [28], in other studies, it has been noted that the Li diffusion is either based on pure single-jumps or a mixed of single-jumps and concerted mechanism [23, 19, 37]. The reported energy barrier for Li migration in c-LLZO is in the range of 0.19-0.33 eV

[34, 23, 38, 39, 40]. Li migration in LGPS has been reported to follow highly correlated motions of Li ions which is ultra-fast in 1 dimension (along the *c*-axis) and fast in 2 dimensions (within the *ab*-plane) with the energy barrier in the range of 0.17-0.23 eV. [41, 42, 18, 43].

The influence of external strain on Li migration has been previously investigated in LLZO [24, 27] and LGPS [44, 45]. An *ab initio* molecular dynamics (AIMD) study by Andriyevsky *et al.* [24] on tetragonal LLZO shows that a 10% compressive strain decreases the diffusion coefficient by 50%. Andriyevsky *et al.* have related this effect to the reduced D_0 value since they showed that the energy barrier even decreases by 5%. AIMD simulation by Miara *et al.* [27] has demonstrated that 5% compression of lattice parameters reduces the conductivity by almost one order of magnitude in c-LLZO at 1000 K. They have related this reduction in conductivity to increase in Li migration barrier due to a contraction of the triangle diffusion bottleneck [27]. However in another study, Zhang *et al.* [39] have recently investigated the effect of Zr substitution on the bottleneck size and migration energy of Li in c-LLZO. Substitution of Zr with tetravalent elements which have different ionic radius can affect the size of migration bottleneck by changing O–O bond lengths. Surprisingly, they have indicated that a dopant that has a smaller size than Zr decreases the bottleneck size, which can lower the Li migration energy. They have emphasized that larger bottleneck size is not necessarily in favor of Li^+ migration. These results are in contrast to the previous findings of Andriyevsky *et al.* [24] and Miara *et al.* [27]. It should be noted that the large compressive strains considered by Andriyevsky *et al.* [24] and Miara *et al.* [27] might lead to disordering of atomic arrangement and different results compared to that reported by Zhang *et al.* [39] in LLZO. In an AIMD study by Ong *et al.* [44], ±4% strains were applied to LGPS and the resulting variation of Li diffusion coefficient and energy barrier was evaluated. They found that the Li migration barrier increases by more than two times, *i.e.* from 0.23 eV to 0.59 eV, upon a –4% (compressive) strain. However, Chen *et al.* [45] reported that the Li migration barrier in LGPS decreases only from 0.26 eV to 0.18 eV upon a very strong strain of +12% along the *c*-axis direction and from 0.31 eV to 0.15 eV upon +12% strain in the *ab*-plane.

The concept of elastic dipole method (EDM) [46, 47] has been applied to predict the

effect of external strain on formation and migration energy of point defects in various materials [48, 49, 50, 51, 52, 53]. Our recent studies [52, 53], for example, have shown that in $LiCoO_2$, as one of the most commonly-used layered cathode material in Li-ion batteries, a 1% compressive (tensile) in-plane strain can change the formation energy of Li^+ vacancy by almost –0.04 eV (+0.04 eV) [52]. We have also shown that a 1% compressive (tensile) out-of-plane strain increases (decreases) the migration barrier of Li ion vacancy by about 0.07 eV (0.06 eV) [52]. It should be noted that the results of direct method and EDM in our studies for $LiCoO_2$ [52, 53] are in fair agreement.

Here, we investigate the possibility of applying EDM for predicting Li defect formation energy and migration barrier in Al-LLZO and LGPS solid electrolytes. A comparison between EDM and the direct method (manually applying strain) is given. Moreover, effect of doping-induced strain on the migration barrier of Li^+ ions is calculated and compared to the predicted values from EDM and direct methods.

2. Computational Details

Density functional theory (DFT) calculations and AIMD simulations were performed using the Vienna *ab initio* simulation package (VASP) [54, 55] with the projector augmented-wave pseudopotential approach [56, 57]. The PBE exchange-correlation functional [58] was applied to compute the total energies, stresses, migration barriers (using climbing nudged elastic band (Cl-NEB) with 8 images), and diffusion coefficients (AIMD). The convergence criteria for electronic self-consistency and geometry steps were 10^{-5} eV and 10^{-4} eV/Å, respectively. All the DFT calculations were spin-polarized. A plane wave cutoff energy of 500 eV was used for all DFT and AIMD calculations. Sampling of the Brillouin zone was performed using the following k-point meshes: i) DFT: 2×2×2 for c-, Al-, and Ta-LLZO, 3×2×2 for LGPS; ii) AIMD: 1×1×1 for c-, Al-, and Ta-LLZO, 3×2×2 for LGPS. The lattice parameters of the optimized structures (see Fig. 1) are listed in Tab. 1.

The AIMD calculations were performed in the NVT ensembles from 800 K to 1600 K (interval of 200 K) for 40-50 ps with a time step of 1 fs. The mean squared displace-

ment (MSD) was calculated form AIMD simulations using the following equation

$$\mathrm{MSD}(\tau) = \frac{1}{N_{\mathrm{Li}}} \sum_i |r_i(\tau + t) - r_i(t)|^2. \tag{1}$$

Here, N_{Li} is the total number of mobile Li ions. $r_i(t)$ is the position of the i^{th} Li ion at time t, while τ is an interval of time taken by the ion to walk from $r_i(t)$ to $r_i(\tau + t)$. The diffusion coefficients were then calculated using

$$D_{\mathrm{Li}} = \lim_{\tau \to \infty} \frac{\mathrm{MSD}(\tau)}{2d\tau}, \tag{2}$$

where d is the dimensionality of diffusion (*i.e*. equal to 3 for LGPS and LLZO structures). The diffusion energy barrier was obtained from the slope of Ln(D) plot versus the inverse of $k_{\mathrm{B}}T$.

The Li-ionic conductivity was then determined by

$$\sigma_{\mathrm{Li}} \quad = \frac{q^2 F^2}{\mathrm{RT}} n_{\mathrm{Li}} D_{\mathrm{Li}}, \tag{3}$$

where q, F, R, and T are charge of the carrier, Faraday constant, gas constant, and temperature, respectively. n_{Li} is the volumetric concentration of charge carriers (Li ions) in the solid electrolyte.

The atomic structures and AIMD trajectories were visualized using VESTA [59] and OVITO [60] programs, respectively. The MSD calculations were performed using the python interface in OVITO.

3. RESULTS AND DISCUSSION

Defect formation energies of most probable point defects have to be first calculated to explore the thermodynamics of defects in Al-LLZO and LGPS. We have recently

Table 1: Optimized lattice parameters (using DFT-PBE) of 1×1×1 unit cells of c-LLZO, Al-LLZO, Ta-LLZO, and LGPS in Å. The atomic structures of Al-LLZO and LGPS are illustrated in Fig. 1

Structure	c-LLZO	Al-LLZO	Ta-LLZO	LGPS
a	12.932	12.986	12.940	8.851
b	13.056	13.022	13.068	8.719
c	13.087	13.022	13.030	12.809

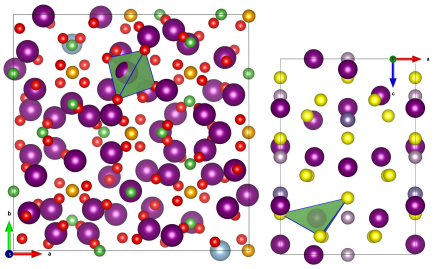

Figure 1: Atomic structures of Al-LLZO (left) and LGPS (right). As an example, in each structure, one Li-contained tetrahedral containing a bottleneck area for Li diffusion is shown in green. Li, Al, Zr, La, O, and S are indicated with magenta, blue, gold, green, red and yellow, respectively. At this view, Ge ions in LGPS are not visible.

reported the formation energies of a variety of possible defect types in unstrained Al-LLZO [14]. It was shown that a Li Frenkel pair is the dominant type of defect in this system. In this work, we calculated the formation energies of all possible point defects in an unstrained bulk LGPS using the following equation (same approach used in Ref. [14]):

$$\Delta E_{\mathrm{d}}^{i,q} = E_{\mathrm{tot}}^{\mathrm{d}} - E_{\mathrm{tot}}^{\mathrm{p}} + n_i\mu_i + q(\epsilon_{\mathrm{F}} + \epsilon_{\mathrm{VBM}}) + \Delta E_{\mathrm{cor}} \qquad (4)$$

$$i = \mathrm{Li},\ \ \mathrm{Ge},\ \ \mathrm{P},\ \ \mathrm{S},$$

where $E_{\mathrm{tot}}^{\mathrm{d}}$ and $E_{\mathrm{tot}}^{\mathrm{p}}$ are the total energies of defective and pristine structures, respectively. n_i, ϵ_F, and ΔE_{cor} are, respectively, the number of defects (+ for vacancy and – for interstitial defects) in the supercell, Fermi level (referenced to the bulk valence-band maximum (VBM) energy (ϵ_{VBM}), and alignment of electrostatic potentials of defective and pristine supercells as well as the correction of finite-cell size effect. $\mu_i(=\mu_i^0 + \Delta\mu_i)$ is the chemical potential of defects referenced to the ground state chemical potential μ_i^0, which is equal to the total energy per atom of the reservoirs, *i.e.* Li, Ge, and P bulks as well as molecular S_8. $\Delta\mu_i$ is considered to be within the range of possible chemical potentials where LGPS is thermodynamically stable, which was extracted from the DFT study by Oh *et al.* [16]. Our defect formation energy results, in agreement with the theoretical study of Oh *et al.* [16], show that interstitial and vacant charged Li ions are of favorable defect types in LGPS under the charge neutrality condition.

Calculated values of Li defect formation energies as function of $\Delta\mu_{\mathrm{Li}}$ for Al-LLZO (see the computational details in ref. [14]) and LGPS are illustrated in Fig. 2. For the Al-LLZO system with a large band gap (BG) of 5.8 eV [14], the values of ΔE_{d} for the entire range of possible $\Delta\mu_{\mathrm{Li}}$ do not vary with $\Delta\mu_{\mathrm{Li}}$. As explained in ref. [14], the reason for this behavior is that the Fermi energy changes linearly with $\Delta\mu_{\mathrm{Li}}$ with a slope of 1. Therefore, the $n_i\Delta\mu_{\mathrm{Li}} + q_i\epsilon_{\mathrm{F}}$ term in Eq. 4 becomes a constant value since $q_i = -n_i$ for a Li defect with a charge state of ± 1 and a dilute concentration of $n_i = \mp 1$ in a large supercell. However, for the LGPS system with a small BG of 2.9 eV [16], the values of ΔE_{d} are constant only for a narrow range of $-2.27 \leq \Delta\mu_{\mathrm{Li}} \leq -2.22$. Our calculated values of ΔE_{d} for $\mathrm{V}^{-}_{\mathrm{Li}}$ and $\mathrm{Li}^{+}_{\mathrm{Li}}$ in LGPS at $\Delta\mu_{\mathrm{Li}} = -2.27$eV are +0.22 and +0.27 eV, respectively. These values are in fair agreement with the value of +0.19 eV for $\mathrm{V}^{-}_{\mathrm{Li}}$ and +0.24 eV for $\mathrm{Li}^{+}_{\mathrm{Li}}$ reported by Oh *et al.* [16] at a Fermi level of 1.51 eV. Based on our results, the formation energies of V_{Li} and $\mathrm{Li}^{+}_{\mathrm{Li}}$ are much lower in Al-LLZO [14] than those in LGPS.

To calculate the effect of external strain on the formation energy of Li defects and migration barrier of Li ions, we used the direct approach and EDM. In the former method, we applied compressive and tensile strains (up to $\pm 2\%$) to the supercells directly and calculated the formation energies and migration barriers. Within EDM,

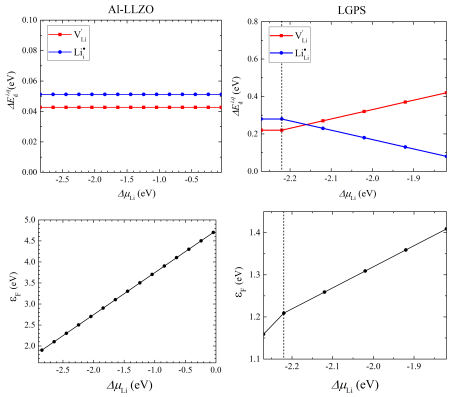

Figure 2: Formation energies of charged Li vacancy ($\mathrm{V}'_{\mathrm{Li}}$) and interstitial Li ($\mathrm{Li}^{\bullet}_{\mathrm{Li}}$) as a function of the Li chemical potential in Al-LLZO (left) and LGPS (right). Fermi energy as a function of Li chemical potential in Al-LLZO and LGPS is plotted for each case. The charge-neutrality condition is preserved by considering all possible defect types, but here, $\Delta E^{i,q}_{\mathrm{d}}$ only for Li defects are presented. $\Delta E^{i,q}_{\mathrm{d}}$ and ϵ_{F} values for Al-LLZO are from ref. [14]

energy of a system with a defect density of $n_\mathrm{d} = N_\mathrm{d}/V$ under a strain field of ϵ_{ij} is expanded by

$$
\begin{aligned}
E(n_\mathrm{d}, \epsilon) = E_0 + \sum_{i,j} \underbrace{\frac{\partial E}{\partial \epsilon_{ij}}}_{\sigma_{ij}=0} \epsilon_{ij} + \frac{1}{2} \sum_{i,j,k,l} \underbrace{\frac{\partial^2 E}{\partial \epsilon_{ij} \partial \epsilon_{kl}}}_{C_{ijkl} \sim \text{const.}} \epsilon_{ij}\epsilon_{kl} + \\
\underbrace{\frac{\partial E}{\partial n_\mathrm{d}}}_{E_\mathrm{d}} n_\mathrm{d} + \sum_{i,j} \underbrace{\frac{\partial^2 E}{\partial n_\mathrm{d} \partial \epsilon_{ij}}}_{-G_{ij}} \epsilon_{ij} n_\mathrm{d} + \dots \\
= E_0 + \frac{1}{2} \sum_{i,j,k,l} C_{ijkl}\epsilon_{ij}\epsilon_{kl} + n_\mathrm{d} \left(E_\mathrm{d} - \sum_{i,j} G_{ij}\epsilon_{ij} \right) + \dots
\end{aligned}
\tag{5}
$$

In Eq. 5, the first term is the total energy of the pristine strain-free structure. The second term is zero since we assume that the defect-free system is fully relaxed and is stress-free. In the third term we have elastic constants of the material which is assumed to remain unchanged after creating a defect in the structure. This is justified by the fact that n_d is very small. The forth term contains the defect formation energy. The fifth term contains the so-called elastic dipole tensor (G_{ij}) which is defined as the negative derivative of the defect formation energy E_d with respect to strain [52, 46, 47]

$$
G_{ij} = -\frac{\partial E_d}{\partial \epsilon_{ij}}. \tag{6}
$$

The formation energy of a defect as function of an external strain can then be estimated by

$$
\Delta E^{i,q}_\mathrm{d}(\epsilon_{ij}) = \Delta E^{i,q}_{\mathrm{d}(0)} - \sum_{ij} G_{ij}\epsilon_{ij}, \tag{7}
$$

where $\Delta E^{i,q}_{\mathrm{d}(0)}$ is the defect formation energy in the unstrained system.

Therefore, elastic dipole tensor can couple the formation energy of point defects to the external strain. For instance, applying a tensile strain reduces the formation energy of a defect with a positive relaxation volume and vice versa. To evaluate G_{ij} in terms

of stress, we write the defect-induced stress in the system as

$$\sigma_{ij}^{\mathrm{d}} \equiv \frac{\partial E(n_{\mathrm{d}}, \epsilon_{ij})}{\partial \epsilon_{ij}} = \sum_{kl} C_{ijkl}\epsilon_{kl} - n_{\mathrm{d}} G_{ij} = \sigma_{ij}^{0} - n_{\mathrm{d}} G_{ij}. \tag{8}$$

In this equation, σ_{ij}^{d} and σ_{ij}^{0} are the stresses of the defective and pristine systems, respectively. The elastic dipole tensor can then be calculated using the following equation by considering that the ionic positions can be relaxed but the lattice parameters are fixed

$$G_{ij} = -\left.\frac{\partial \sigma_{ij}}{\partial n_{\mathrm{d}}}\right|_{\epsilon_{ij}} = -\frac{1}{n_{\mathrm{d}}}(\sigma_{ij}^{\mathrm{d}} - \sigma_{ij}^{0}) = -V_0 \Delta\sigma_{ij} \tag{9}$$

where V_0 is the volume of supercell with a single defect.

The migration barrier is computed by subtraction of energy of system at initial state (IS) from that at transition state (TS):

$$\Delta E_{\mathrm{b}}(\epsilon_{ij}) = E^{\mathrm{TS}}(\epsilon_{ij} = 0) - E^{\mathrm{IS}}(\epsilon_{ij} = 0) - \sum_{ij} G_{ij}^{\mathrm{TS}} \epsilon_{ij} \tag{10}$$

where $E^{\mathrm{TS}}(\epsilon_{ij} = 0)$ and $E^{\mathrm{IS}}(\epsilon_{ij} = 0)$ are the total energy of TS and IS in the unstrained material. G_{ij}^{TS} is the elastic dipole tensor at TS with respect to IS. The atomic

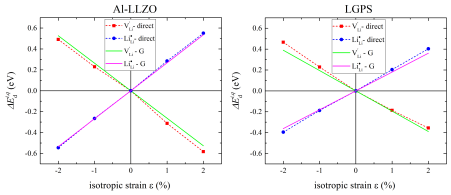

Figure 3: Formation energies of charged Li vacancy (V'_{Li}) and interstitial Li ($Li^{\bullet}_{Li}$) in Al-LLZO and LGPS as function of isotropic strain calculated using the direct approach and EDM. The values are referenced to $\Delta E_{\mathrm{d}}^{i,q}$= +0.042 eV and +0.051 eV for V'_{Li} and $Li^{\bullet}_{Li}$ in Al-LLZO, respectively, $\Delta E_{\mathrm{d}}^{i,q}$= +0.22 eV and +0.27 eV for V'_{Li} and $Li^{\bullet}_{Li}$ in LGPS, respectively.

Table 2: Li-defect-induced variation of volume with respect to the pristine Al-LLZO and LGPS structures. Positive and negative signs indicate expansion and contraction, respectively.

Defective structure	Change in the volume ΔV (in %)
V'_{Li} (Al-LLZO)	+0.56
$Li^{\bullet}_{Li}$ (Al-LLZO)	–0.54
V'_{Li} (LGPS)	+5.35
$Li^{\bullet}_{Li}$ (LGPS)	–4.17

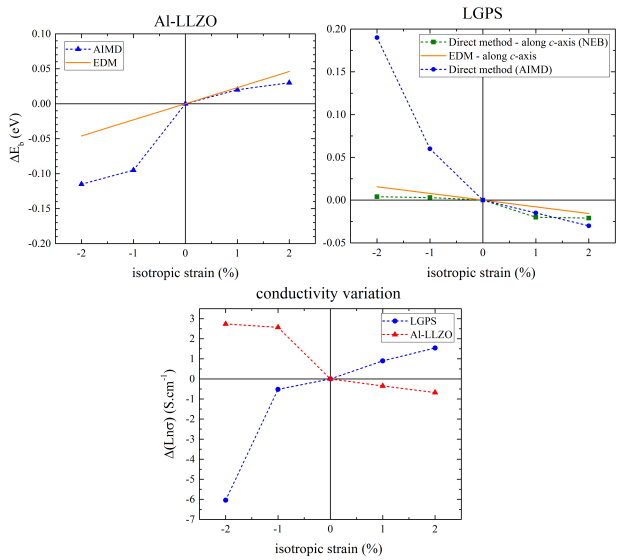

Figure 4: Calculated variations of the migration-barrier (left and middle) and conductivity (right) with isotropic strain in Al-LLZO and LGPS. In the left figure, the results from the direct method (AIMD simulation) and EDM (only for one diffusion channel) are plotted. In the middle figure, the results from the direct method (NEB calculations) and EDM for one diffusion channel (along the c-axis) as well as the direct method (AIMD simulation) for LGPS are presented. In the right figure, the diffusion coefficients that are needed to calculate Li ionic conductivities are obtained from the AIMD simulations.

coordinates of the TS which are needed to calculate G_{ij}^{TS} are obtained from the NEB calculation of the unstrained case.

The calculated formation energies of $\mathrm{V}_{\mathrm{Li}}^{-}$ and $\mathrm{Li}_{\mathrm{Li}}^{+}$ in Al-LLZO and LGPS as function of strain are illustrated in Fig. 3. The calculated values of ΔE_{d} within EDM (using Eq. 7) are in fair agreement with those of the direct method. In all four cases, the deviation between the direct and EDM results becomes greater for larger strains since it approaches towards the non-elastic regime. For both electrolyte materials, a tensile

Table 3: Calculated average migration barriers (in eV) and conductivity (in S.cm^{-1}) in pure c-LLZO, Al-doped LLZO, Ta-doped LLZO, and LGPS using AIMD simulations corresponding to Figs. 5 and 6.

System	$\Delta E_{\mathrm{b}}(\epsilon = 0)$	σ at RT
c-LLZO	0.30	4.6×10^{-6}
Al-LLZO	0.37	5.6×10^{-7}
Ta-LLZO	0.20	6.7×10^{-5}
LGPS	0.23	1.5×10^{-4}

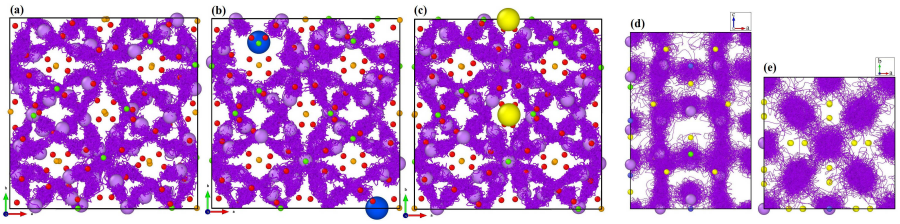

Figure 5: Integrated Li ion trajectories for (a) c-LLZO, (b) Al-LLZO, (c) Ta-LLZO and (e, f) pristine LGPS at 1200 K. Li ions and their pathways are in magenta color. Al and Ta dopants are indicated with blue and yellow colors, respectively.

strain leads to a decrease in ΔE_{d} of $\mathrm{V}_{\mathrm{Li}}^{-}$. This is due the fact that the formation of $\mathrm{V}_{\mathrm{Li}}^{-}$ tends to expand the lattice parameters (see Tab. 2). However, formation of $\mathrm{Li}_{\mathrm{Li}}^{+}$ tends to shrink the lattice parameters (see Tab. 2), and, for this reason, a compressive strain leads to a decrease in the formation energy of $\mathrm{Li}_{\mathrm{Li}}^{+}$. Effect of strain on formation energy of Li defects is found to be larger in Al-LLZO than in LGPS. Percentage of the defect-induced variation of volume is larger in LGPS than in Al-LLZO (see Tab. 2) since the defect-free lattice parameters of the former case are shorter (see Tab. I).

To study the effect of strain on migration barrier, we first started with LGPS since the degree of atomic displacements and disordering upon Li transport is smaller in this system than in Al-LLZO. Considering Li migration along the *c*-axis direction (see Fig. 5(d)), we calculated diffusion barrier using DFT-Cl-NEB for different lattice parameter values (i.e. compressive and tensile strains between -2% and $+2\%$). Fig. 4 shows that the migration barrier $\Delta E_{\mathrm{b}}(\epsilon)$ increases only slightly (less than 5 meV) by compressive strains. However, $\Delta E_{\mathrm{b}}(\epsilon)$ decreases more significantly with tensile strains. Nevertheless, the change in the barrier is very small, i.e. less than 22 meV for strain values between -2% and $+2\%$. Although both the EDM and direct method show that ΔE_{b} increases (decreases) with compressive (tensile) strain, the values calculated using the former method are not quantitatively in agreement with those computed using the latter one. Therefore, EDM can not accurately describe the effect of strain in complex electrolyte systems. However, as we will discuss later, EDM can help us to understand the trend in variation of migration barrier as function of strain.

We continued our study with applying AIMD simulations to estimate the average

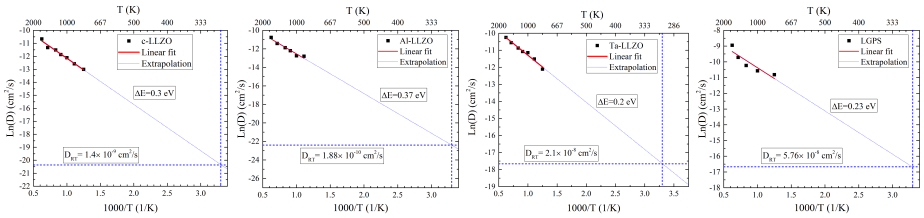

Figure 6: Arrhenius plots of diffusion coefficients in pure c-LLZO, Al-doped LLZO, Ta-doped LLZO, and LGPS. Calculated Li migration barrier and diffusion coefficient for room temperature at each case is shown.

diffusion barrier as function of strain for Al-LLZO and LGPS systems. The integrated Li trajectories in Al-LLZO and LGPS are illustrated in Fig. 5(a)-(e). It can be seen from the trajectories that the diffusion pathways in Al-LLZO and LGPS are in 3D. In LGPS, although the migration barrier along the *c*-axis is lower (ultra-fast) compared to the *ab*-plane (fast), lots of Li jumps can be seen in the *ab*-plane which shows its contribution to the whole diffusion process. This finding has also been reported in previous studies [41, 42, 18, 43]. Besides Al-LLZO, we performed AIMD simulation for pristine and Ta-doped c-LLZO. These calculations can help us to investigate effect of doping-induced lattice size change on Li migration barrier in c-LLZO. Figure 5-b clearly shows depletion of Li ions close to the Al cations. However, in the case of Ta-LLZO, we observe larger Li migration even compared to c-LLZO. Thus, the (averaged) diffusion barriers are calculated to be as the following order (Table 3): $\Delta E_{\mathrm{b}}(\mathrm{Ta-LLZO}) < \Delta E_{\mathrm{b}}(\mathrm{c-LLZO}) < \Delta E_{\mathrm{b}}(\mathrm{Al-LLZO})$.

The calculated values of ΔE_{b} as function of strain (Fig. 4) show that a compressive

Table 4: Average area as well as variation in area of bottleneck of Li diffusion pathway. Positive and negative signs indicate expansion and contraction, respectively. The bottleneck area in Al-LLZO and LGPS are referred to the one triangle of O or S tetrahedrals, respectively.

System	Strain		
Al-LLZO	–2%	0%	+2%
Absolute values (in Å^2)	4.16	4.33	4.51
Change in values (in %)	–4.01	0	+3.99
System	Strain		
Pristine LGPS	–2%	0%	2%
Absolute values (in Å^2)	6.29	6.56	6.84
Change in values (in %)	–4.06	0	+4.15

strain lowers the migration barrier in Al-LLZO, while it enhances it in LGPS. A similar behavior to what we found in LGPS [45, 44] has been also reported for ion migration in many other ionic crystals such as $LiCoO_2$, UO_2, $SrTiO_3$, and several perovskite-structured oxygen conductors [52, 48, 61, 62, 63, 64]. A compressive strain leads to narrowing of bottleneck width of Li diffusion (see Tab. 4) and increasing of diffusion barrier in LGPS. Although a compressive strain also reduces the width of bottleneck of Li migration in Al-LLZO (see Tab. 4), but it does not suppress Li diffusion as it has been also reported by Zhang *et al.* [39].

Based on EDM results, this behavior is due to the tendency of lattice size and Li–O bond lengths to contract at TS (at the bottleneck). This can be seen in Tab. 5 showing large compressive stresses in two directions. However, in the case of LGPS, the lattice sizes and Li–S tend to expand, which, as can be seen in Tab. 5, tensile stresses arise in three direction at TS of Li migration in LGPS.

Regarding the effect of doping on Li transport in c-LLZO, we find that two parameters control the averaged migration barrier: i) site preference for dopant (local effect) and ii) lattice parameter change (global effect). Occupation of Li sites by cation dopant suppresses Li migration significantly since Li ions are repelled by the large positive charge on the dopant. For this reason, in spite of volume contraction of 0.27% and more 4 Li vacant sites per unitcell, the average migration barrier in Al-LLZO is 0.07 eV higher than that in c-LLZO, which is due to the blocking of Li pathway by Al cations that are located in Li sites. The contraction of unitcell of Al-LLZO can be understood by comparing the ionic radius of Al^{3+} (0.67 Å) compared to Li^{+} (0.90 Å). However, if the dopant occupies the other site types, the global effect plays a key role in determining of the migration barrier. The example is Ta dopant which occupies Zr site. Assuming the effect of strain on bottleneck width and migration barrier in c-LLZO to

Table 5: Arising isotropic stresses at the transition state point for one migration pathway in Al-LLZO and LGPS. Negative and positive values indicate compressive and tensile stresses, respectively. All values are in kBar.

System	P_{xx}	P_{yy}	P_{zz}
Al-LLZO	–1.17	–1.36	+0.86
LGPS	+0.50	+0.25	+0.41

Table 6: Volume change (in percent) upon doping of c-LLZO with Al and Ta. The reference volume is c-LLZO. Positive and negative signs indicate expansion and contraction, respectively.

dopant	Al-LLZO	Ta-LLZO
ΔV (in %)	–0.27	–0.22

be similar to that in Al-LLZO, we estimated the effect of Ta-doping on the Li migration barrier in c-LLZO as follows. Tab. 6 indicates that a Ta-doping of 12.5% (with respect to total 16 Zr ions in the conventional unit cell of c-LLZO in Fig.1) in c-LLZO shrinks the volume by 0.22%, which is about an isotropic strain of –0.6%. In spite of formation of 2 V'_{Li}, the unitcell volume of Ta-LLZO is smaller than that of c-LLZO, which is due to the small size of Ta^{5+} (0.78 Å) compared to Zr^{4+} (0.86 Å). Figure 4 shows that a compressive strain of –1% decreases the migration barrier in Al-LLZO (or c-LLZO) by 0.1 eV. Calculated migration barrier for Ta-LLZO in Fig. 6 is 0.2 eV which is also 0.1 eV lower than that for strain-free c-LLZO. The dopant-induced (isotropic) compressive strain in Ta-LLZO is 0.4% smaller than the compressive strain of –1% that has been considered to compute ΔE_b in Fig. 4. However, calculated ΔE_b in Ta-LLZO is similar to that in Al-LLZO with a –1% strain. The further decrease in the migration barrier for Ta-LLZO, in spite of smaller compressive strain than –1%, can be due to the more number of vacant Li sites in Ta-LLZO compared to c-LLZO.

Calculated variation of ionic conductivity (σ_{Li}) with strain (Fig. 4) shows that a compressive strain of –2% can enhance σ_{Li} by 1 order of magnitude in LLZO. However, a tensile strain of 2% can reduce σ_{Li} by a factor of about 0.5. Nevertheless, a tensile strain of 2% can enhance σ_{Li} of LGPS by a factor of 5, while a compressive strain of –2% reduces σ_{Li} by 2 orders of magnitude.

4. CONCLUSION

In this article, we have studied the effect of strain on formation energy of Li defects as well as migration barrier of Li ions in complex solid electrolyte materials such as Al-LLZO and and LGPS. In particular, we investigated whether a computationally efficient approach, the elastic dipole method EDM, can be applied to predict impact of strain on the aforementioned quantities. It was found that this method can predict

the strain dependency of formation energy of charged interstitial Li ($Li^{\bullet}_{Li}$) and Li vacancy (V'_{Li}) in Al-LLZO and LGPS with a reasonable accuracy. In both systems, a compressive strain makes formation of $Li^{\bullet}_{Li}$ more favorable, while V'_{Li} less favorable. Furthermore, we found that EDM can not quantitatively predict the impact of an external strain on Li migration barrier. Nevertheless, it can qualitatively predict whether the barrier would decrease or increase by applying a strain field. Our further AIMD simulation shows that the effect of strain on Li migration in LGPS is similar to simple ionic crystals such as LCO where a compressive strain increase the energy barrier due to the contraction of the bottleneck width of Li diffusion. However, in agreement with a recent experimental report, we found that a compressive strain decreases the bottleneck width but it lowers the migration barrier in Al-LLZO. Our further calculations indicate that we can predict effect of doping on Li migration barrier in solid electrolytes if we have a plot of migration barrier as a function of strain. For example, when a Zr cation is replaced by Ta dopant, the lattice parameter of c-LLZO contracts. This global effect of Ta-doping contracts the bottleneck width of Li migration leading to the decrease in the migration barrier in c-LLZO. However, for the case of Al-LLZO, where Al ions sit at Li sites, the local effect of Li blocking plays the key role in Li transport resulting in increase in the migration barrier in c-LLZO. Finally, we showed that the impact of strain on the value of Li ionic conductivity of solid electrolyte materials can be as large as 2 orders of magnitude.

5. Acknowledgement

The authors acknowledge the funding support from the German Research Foundation (DFG) of the project number 383045781 as well as the computing time granted on the Hessian high performance computer “LICHTENBERG” and high performance computing center in Stuttgart (HLRS). We also acknowledge supports by Joachim Maier and Eugene Kotomin from Max Planck Institute for Solid State Research in Stuttgart.

References

[1] Z. Zhang, Y. Shao, B. Lotsch, Y.-S. Hu, H. Li, J. Janek, L. F. Nazar, C.-W. Nan, J. Maier, M. Armand, L. Chen, New horizons for inorganic solid state ion conductors, Energy & Environmental Science 11 (8) (2018) 1945–1976. doi:10.1039/c8ee01053f.
URL https://doi.org/10.1039/c8ee01053f

[2] J. B. Goodenough, Rechargeable batteries: challenges old and new, Journal of Solid State Electrochemistry 16 (6) (2012) 2019–2029.

[3] J. Garcia-Barriocanal, A. Rivera-Calzada, M. Varela, Z. Sefrioui, E. Iborra, C. Leon, S. J. Pennycook, J. Santamaria, Colossal ionic conductivity at interfaces of epitaxial ZrO2:y2o3/SrTiO3 heterostructures, Science 321 (5889) (2008) 676–680. doi:10.1126/science.1156393.
URL https://doi.org/10.1126/science.1156393

[4] C. Korte, J. Keppner, A. Peters, N. Schichtel, H. Aydin, J. Janek, Coherency strain and its effect on ionic conductivity and diffusion in solid electrolytes – an improved model for nanocrystalline thin films and a review of experimental data, Phys. Chem. Chem. Phys. 16 (44) (2014) 24575–24591. doi:10.1039/c4cp03055a.
URL https://doi.org/10.1039/c4cp03055a

[5] N. Schichtel, C. Korte, D. Hesse, J. Janek, Elastic strain at interfaces and its influence on ionic conductivity in nanoscaled solid electrolyte thin films—theoretical considerations and experimental studies, Physical Chemistry Chemical Physics 11 (17) (2009) 3043. doi:10.1039/b900148d.
URL https://doi.org/10.1039/b900148d

[6] H. Liu, Q. Cao, L. Fu, C. Li, Y. Wu, H. Wu, Doping effects of zinc on LiFePO4 cathode material for lithium ion batteries, Electrochemistry Communications 8 (10) (2006) 1553–1557. doi:10.1016/j.elecom.2006.07.014.
URL https://doi.org/10.1016/j.elecom.2006.07.014

[7] H. Tukamoto, Electronic conductivity of LiCoO[sub 2] and its enhancement by magnesium doping, Journal of The Electrochemical Society 144 (9) (1997) 3164. doi:10.1149/1.1837976.
URL https://doi.org/10.1149/1.1837976

[8] J. Jamnik, J. Maier, Nanocrystallinity effects in lithium battery materials, Physical Chemistry Chemical Physics 5 (23) (2003) 5215. doi:10.1039/b309130a.
URL https://doi.org/10.1039/b309130a

[9] R. Mukherjee, R. Krishnan, T.-M. Lu, N. Koratkar, Nanostructured electrodes for high-power lithium ion batteries, Nano Energy 1 (4) (2012) 518–533. doi:10.1016/j.nanoen.2012.04.001.
URL https://doi.org/10.1016/j.nanoen.2012.04.001

[10] S. S. Gundale, A. Deshpande, Improvement of ionic conductivity in li 3.6 si 0.6 v 0.4 o 4 ceramic inorganic electrolyte by addition of LiBO 2 glass for li ion battery application, Electrochimica Acta 265 (2018) 65–70. doi:10.1016/j.electacta.2018.01.122.
URL https://doi.org/10.1016/j.electacta.2018.01.122

[11] W. Fan, X. Liu, Z. Wang, P. Fei, R. Zhang, Y. Wang, C. Qin, W. Zhao, Y. Ding, Synergetic enhancement of the electronic/ionic conductivity of a li-ion battery by fabrication of a carbon-coated nanoporous SnOxSb alloy anode, Nanoscale 10 (16) (2018) 7605–7611. doi:10.1039/c8nr00550h.
URL https://doi.org/10.1039/c8nr00550h

[12] X. Zhan, S. Lai, M. P. Gobet, S. G. Greenbaum, M. Shirpour, Defect chemistry and electrical properties of garnet-type li7la3zr2o12, Physical Chemistry Chemical Physics 20 (3) (2018) 1447–1459. doi:10.1039/c7cp06768b.
URL https://doi.org/10.1039/c7cp06768b

[13] M. Kubicek, A. Wachter-Welzl, D. Rettenwander, R. Wagner, S. Berendts, R. Uecker, G. Amthauer, H. Hutter, J. Fleig, Oxygen vacancies in fast lithium-ion conducting garnets, Chemistry of Materials 29 (17) (2017) 7189–7196.

doi:10.1021/acs.chemmater.7b01281.
URL https://doi.org/10.1021/acs.chemmater.7b01281

[14] A. Moradabadi, P. Kaghazchi, Defect chemistry in cubic li6.25al0.25la3zr2o12 solid electrolyte: A density functional theory study, Solid State Ionics 338 (2019) 74–79. doi:10.1016/j.ssi.2019.04.023.
URL https://doi.org/10.1016/j.ssi.2019.04.023

[15] S. KC, R. C. Longo, K. Xiong, K. Cho, Point defects in garnet-type solid electrolyte (c-li7la3zr2o12) for li-ion batteries, Solid State Ionics 261 (2014) 100–105. doi:10.1016/j.ssi.2014.04.021.
URL https://doi.org/10.1016/j.ssi.2014.04.021

[16] K. Oh, D. Chang, B. Lee, D.-H. Kim, G. Yoon, I. Park, B. Kim, K. Kang, Native defects in li10gep2s12 and their effect on lithium diffusion, Chemistry of Materials 30 (15) (2018) 4995–5004. doi:10.1021/acs.chemmater.8b01163.
URL https://doi.org/10.1021/acs.chemmater.8b01163

[17] D. A. Weber, A. Senyshyn, K. S. Weldert, S. Wenzel, W. Zhang, R. Kaiser, S. Berendts, J. Janek, W. G. Zeier, Structural insights and 3d diffusion pathways within the lithium superionic conductor li10gep2s12, Chemistry of Materials 28 (16) (2016) 5905–5915. doi:10.1021/acs.chemmater.6b02424.
URL https://doi.org/10.1021/acs.chemmater.6b02424

[18] Y. Mo, S. P. Ong, G. Ceder, First principles study of the li10gep2s12 lithium super ionic conductor material, Chemistry of Materials 24 (1) (2011) 15–17. doi:10.1021/cm203303y.
URL https://doi.org/10.1021/cm203303y

[19] K. Meier, T. Laino, A. Curioni, Solid-state electrolytes: Revealing the mechanisms of li-ion conduction in tetragonal and cubic LLZO by first-principles calculations, The Journal of Physical Chemistry C 118 (13) (2014) 6668–6679. doi:10.1021/jp5002463.
URL https://doi.org/10.1021/jp5002463

[20] A. Bhandari, J. Bhattacharya, Origin of fast ion conduction in li10gep2s12, a superionic conductor, The Journal of Physical Chemistry C 120 (51) (2016) 29002–29010. doi:10.1021/acs.jpcc.6b10967.
URL https://doi.org/10.1021/acs.jpcc.6b10967

[21] D. O. Shin, K. Oh, K. M. Kim, K.-Y. Park, B. Lee, Y.-G. Lee, K. Kang, Synergistic multi-doping effects on the li 7 la 3 zr 2 o 12 solid electrolyte for fast lithium ion conduction, Scientific reports 5 (2015) 18053.

[22] Y. Chen, E. Rangasamy, C. Liang, K. An, Origin of high li^+ conduction in doped li7la3zr2o12 garnets, Chemistry of Materials 27 (16) (2015) 5491–5494. doi:10.1021/acs.chemmater.5b02521.
URL https://doi.org/10.1021/acs.chemmater.5b02521

[23] M. Xu, M. S. Park, J. M. Lee, T. Y. Kim, Y. S. Park, E. Ma, Mechanisms of li^+transport in garnet-type cubic $li3^+$xLa3m2o12(m= te, nb, zr), Physical Review B 85 (5). doi:10.1103/physrevb.85.052301.
URL https://doi.org/10.1103/physrevb.85.052301

[24] B. Andriyevsky, K. Doll, T. Jacob, Ab initio molecular dynamics study of lithium diffusion in tetragonal li7la3zr2o12, Materials Chemistry and Physics 185 (2017) 210–217. doi:10.1016/j.matchemphys.2016.10.025.
URL https://doi.org/10.1016/j.matchemphys.2016.10.025

[25] A. Kuhn, J.-Y. Choi, L. Robben, F. Tietz, M. Wilkening, P. Heitjans, Li ion dynamics in al-doped garnet-type li7la3zr2o12crystallizing with cubic symmetry, Zeitschrift für Physikalische Chemie 226 (5-6) (2012) 525–537. doi:10.1524/zpch.2012.0250.
URL https://doi.org/10.1524/zpch.2012.0250

[26] S. Yu, D. J. Siegel, Grain boundary contributions to li-ion transport in the solid electrolyte li7la3zr2o12 (LLZO), Chemistry of Materials 29 (22) (2017) 9639–9647. doi:10.1021/acs.chemmater.7b02805.
URL https://doi.org/10.1021/acs.chemmater.7b02805

[27] L. J. Miara, S. P. Ong, Y. Mo, W. D. Richards, Y. Park, J.-M. Lee, H. S. Lee, G. Ceder, Effect of rb and ta doping on the ionic conductivity and stability of the garnet li7^{+}2x–y(la3–xRbx)(zr2–yTay)o12 ($0 \leq x \leq 0.375$, $0 \leq y \leq 1$) superionic conductor: A first principles investigation, Chemistry of Materials 25 (15) (2013) 3048–3055. doi:10.1021/cm401232r.
URL https://doi.org/10.1021/cm401232r

[28] R. Jalem, Y. Yamamoto, H. Shiiba, M. Nakayama, H. Munakata, T. Kasuga, K. Kanamura, Concerted migration mechanism in the li ion dynamics of garnet-type li7la3zr2o12, Chemistry of Materials 25 (3) (2013) 425–430. doi:10.1021/cm303542x.
URL https://doi.org/10.1021/cm303542x

[29] W. Xia, B. Xu, H. Duan, Y. Guo, H. Kang, H. Li, H. Liu, Ionic conductivity and air stability of al-doped li7la3zr2o12 sintered in alumina and pt crucibles, ACS Applied Materials & Interfaces 8 (8) (2016) 5335–5342. doi:10.1021/acsami.5b12186.
URL https://doi.org/10.1021/acsami.5b12186

[30] J. Han, J. Zhu, Y. Li, X. Yu, S. Wang, G. Wu, H. Xie, S. C. Vogel, F. Izumi, K. Momma, Y. Kawamura, Y. Huang, J. B. Goodenough, Y. Zhao, Experimental visualization of lithium conduction pathways in garnet-type li7la3zr2o12, Chemical Communications 48 (79) (2012) 9840. doi:10.1039/c2cc35089k.
URL https://doi.org/10.1039/c2cc35089k

[31] P. Canepa, J. A. Dawson, G. S. Gautam, J. M. Statham, S. C. Parker, M. S. Islam, Particle morphology and lithium segregation to surfaces of the li7la3zr2o12 solid electrolyte, Chemistry of Materials 30 (9) (2018) 3019–3027. doi:10.1021/acs.chemmater.8b00649.
URL https://doi.org/10.1021/acs.chemmater.8b00649

[32] M. J. Klenk, W. Lai, Finite-size effects on the molecular dynamics simulation of fast-ion conductors: A case study of lithium garnet oxide li7la3zr2o12, Solid

State Ionics 289 (2016) 143–149. doi:10.1016/j.ssi.2016.03.002.
URL https://doi.org/10.1016/j.ssi.2016.03.002

[33] J.-M. Lee, T. Kim, S.-W. Baek, Y. Aihara, Y. Park, Y.-I. Kim, S.-G. Doo, High lithium ion conductivity of li7la3zr2o12 synthesized by solid state reaction, Solid State Ionics 258 (2014) 13–17. doi:10.1016/j.ssi.2014.01.043.
URL https://doi.org/10.1016/j.ssi.2014.01.043

[34] R. Murugan, V. Thangadurai, W. Weppner, Fast lithium ion conduction in garnet-type li7la3zr2o12, Angewandte Chemie International Edition 46 (41) (2007) 7778–7781. doi:10.1002/anie.200701144.
URL https://doi.org/10.1002/anie.200701144

[35] A. Kuhn, S. Narayanan, L. Spencer, G. Goward, V. Thangadurai, M. Wilkening, Li self-diffusion in garnet-type li7la3zr2o12as probed directly by diffusion-inducedLi7spin-lattice relaxation NMR spectroscopy, Physical Review B 83 (9). doi:10.1103/physrevb.83.094302.
URL https://doi.org/10.1103/physrevb.83.094302

[36] Y. Gao, X. Wang, H. Lu, L. Zhang, L. Ma, Q. Fang, Mechanism of lithium ion diffusion in the hexad substituted li7la3zr2o12 solid electrolytes, Solid State Ionics 291 (2016) 1–7. doi:10.1016/j.ssi.2016.04.017.
URL https://doi.org/10.1016/j.ssi.2016.04.017

[37] X. P. Wang, Y. X. Gao, Y. P. Xia, Z. Zhuang, T. Zhang, Q. F. Fang, Correlation and the mechanism of lithium ion diffusion with the crystal structure of li7la3zr2o12 revealed by an internal friction technique, Phys. Chem. Chem. Phys. 16 (15) (2014) 7006–7014. doi:10.1039/c3cp55515a.
URL https://doi.org/10.1039/c3cp55515a

[38] S. R. Yeandel, B. J. Chapman, P. R. Slater, P. Goddard, Structure and lithium-ion dynamics in fluoride-doped cubic li7la3zr2o12 (LLZO) garnet for li solid-state battery applications, The Journal of Physical Chemistry C 122 (49) (2018) 27811–27819. doi:10.1021/acs.jpcc.8b07704.
URL https://doi.org/10.1021/acs.jpcc.8b07704

[39] Y. Zhang, F. Chen, J. Li, L. Zhang, J. Gu, D. Zhang, K. Saito, Q. Guo, P. Luo, S. Dong, Regulation mechanism of bottleneck size on li^+ migration activation energy in garnet-type li7la3zr2o12, Electrochimica Acta 261 (2018) 137–142. doi:10.1016/j.electacta.2017.12.133.
URL https://doi.org/10.1016/j.electacta.2017.12.133

[40] C. Chen, Z. Lu, F. Ciucci, Data mining of molecular dynamics data reveals li diffusion characteristics in garnet li7la3zr2o12, Scientific Reports 7 (1). doi:10.1038/srep40769.
URL https://doi.org/10.1038/srep40769

[41] A. Marcolongo, N. Marzari, Ionic correlations and failure of nernst-einstein relation in solid-state electrolytes, Physical Review Materials 1 (2). doi:10.1103/physrevmaterials.1.025402.
URL https://doi.org/10.1103/physrevmaterials.1.025402

[42] M. Xu, J. Ding, E. Ma, One-dimensional stringlike cooperative migration of lithium ions in an ultrafast ionic conductor, Applied Physics Letters 101 (3) (2012) 031901. doi:10.1063/1.4737397.
URL https://doi.org/10.1063/1.4737397

[43] X. Liang, L. Wang, Y. Jiang, J. Wang, H. Luo, C. Liu, J. Feng, In-channel and in-plane li ion diffusions in the superionic conductor li10gep2s12 probed by solid-state NMR, Chemistry of Materials 27 (16) (2015) 5503–5510. doi:10.1021/acs.chemmater.5b01384.
URL https://doi.org/10.1021/acs.chemmater.5b01384

[44] S. P. Ong, Y. Mo, W. D. Richards, L. Miara, H. S. Lee, G. Ceder, Phase stability, electrochemical stability and ionic conductivity of the li10±1mp2x12(m = ge, si, sn, al or p, and x = o, s or se) family of superionic conductors, Energy Environ. Sci. 6 (1) (2013) 148–156. doi:10.1039/c2ee23355j.
URL https://doi.org/10.1039/c2ee23355j

[45] B. Chen, J. Ju, J. Ma, H. Du, R. Xiao, G. Cui, L. Chen, Strain tunable ionic transport properties and electrochemical window of li10gep2s12

superionic conductor, Computational Materials Science 153 (2018) 170–175. doi:10.1016/j.commatsci.2018.06.041.
URL https://doi.org/10.1016/j.commatsci.2018.06.041

[46] M. J. Gillan, The elastic dipole tensor for point defects in ionic crystals, Journal of Physics C: Solid State Physics 17 (9) (1984) 1473–1488. doi:10.1088/0022-3719/17/9/006.
URL https://doi.org/10.1088/0022-3719/17/9/006

[47] C. Varvenne, F. Bruneval, M.-C. Marinica, E. Clouet, Point defect modeling in materials: Couplingab initioand elasticity approaches, Physical Review B 88 (13). doi:10.1103/physrevb.88.134102.
URL https://doi.org/10.1103/physrevb.88.134102

[48] A. Goyal, S. R. Phillpot, G. Subramanian, D. A. Andersson, C. R. Stanek, B. P. Uberuaga, Impact of homogeneous strain on uranium vacancy diffusion in uranium dioxide, Physical Review B 91 (9). doi:10.1103/physrevb.91.094103.
URL https://doi.org/10.1103/physrevb.91.094103

[49] D. A. Freedman, D. Roundy, T. A. Arias, Elastic effects of vacancies in strontium titanate: Short- and long-range strain fields, elastic dipole tensors, and chemical strain, Physical Review B 80 (6). doi:10.1103/physrevb.80.064108.
URL https://doi.org/10.1103/physrevb.80.064108

[50] R. Nazarov, J. S. Majevadia, M. Patel, M. R. Wenman, D. S. Balint, J. Neugebauer, A. P. Sutton, First-principles calculation of the elastic dipole tensor of a point defect: Application to hydrogen inα-zirconium, Physical Review B 94 (24). doi:10.1103/physrevb.94.241112.
URL https://doi.org/10.1103/physrevb.94.241112

[51] P. Stein, A. Moradabadi, M. Diehm, B.-X. Xu, K. Albe, The influence of anisotropic surface stresses and bulk stresses on defect thermodynamics in LiCoO2 nanoparticles, Acta Materialia 159 (2018) 225–240. doi:10.1016/j.actamat.2018.07.046.
URL https://doi.org/10.1016/j.actamat.2018.07.046

[52] A. Moradabadi, P. Kaghazchi, J. Rohrer, K. Albe, Influence of elastic strain on the thermodynamics and kinetics of lithium vacancy in bulk LiCoO2, Physical Review Materials 2 (1). doi:10.1103/physrevmaterials.2.015402.
URL https://doi.org/10.1103/physrevmaterials.2.015402

[53] A. Moradabadi, P. Kaghazchi, Effect of strain on polaron hopping and electronic conductivity in bulk LiCoO2, Physical Review Applied 7 (6). doi:10.1103/physrevapplied.7.064008.
URL https://doi.org/10.1103/physrevapplied.7.064008

[54] G. Kresse, J. Furthmüller, Efficient iterative schemes for *ab initio* total-energy calculations using a plane-wave basis set, Physical Review B 54 (16) (1996) 11169–11186. doi:10.1103/physrevb.54.11169.
URL https://doi.org/10.1103/physrevb.54.11169

[55] G. Kresse, J. Furthmüller, Efficiency of ab-initio total energy calculations for metals and semiconductors using a plane-wave basis set, Computational Materials Science 6 (1) (1996) 15–50. doi:10.1016/0927-0256(96)00008-0.
URL https://doi.org/10.1016/0927-0256(96)00008-0

[56] P. E. Blöchl, Projector augmented-wave method, Physical Review B 50 (24) (1994) 17953–17979. doi:10.1103/physrevb.50.17953.
URL https://doi.org/10.1103/physrevb.50.17953

[57] G. Kresse, D. Joubert, From ultrasoft pseudopotentials to the projector augmented-wave method, Physical Review B 59 (3) (1999) 1758–1775. doi:10.1103/physrevb.59.1758.
URL https://doi.org/10.1103/physrevb.59.1758

[58] J. P. Perdew, K. Burke, M. Ernzerhof, Generalized gradient approximation made simple, Physical Review Letters 77 (18) (1996) 3865–3868. doi:10.1103/physrevlett.77.3865.
URL https://doi.org/10.1103/physrevlett.77.3865

[59] K. Momma, F. Izumi, VESTA 3for three-dimensional visualization of crystal, volumetric and morphology data, Journal of Applied Crystallography 44 (6) (2011) 1272–1276. doi:10.1107/s0021889811038970.
URL https://doi.org/10.1107/s0021889811038970

[60] A. Stukowski, Visualization and analysis of atomistic simulation data with OVITO–the open visualization tool, Modelling and Simulation in Materials Science and Engineering 18 (1) (2009) 015012. doi:10.1088/0965-0393/18/1/015012.
URL https://doi.org/10.1088/0965-0393/18/1/015012

[61] H. Grönbeck, V. P. Zhdanov, Effect of lattice strain on hydrogen diffusion in pd: A density functional theory study, Physical Review B 84 (5). doi:10.1103/physrevb.84.052301.
URL https://doi.org/10.1103/physrevb.84.052301

[62] A. Kushima, B. Yildiz, Role of lattice strain and defect chemistry on the oxygen vacancy migration at the (8.3% y, in: ECS Transactions, ECS, 2009. doi:10.1149/1.3205696.
URL https://doi.org/10.1149/1.3205696

[63] F. Ning, S. Li, B. Xu, C. Ouyang, Strain tuned li diffusion in LiCoO2 material for li ion batteries: A first principles study, Solid State Ionics 263 (2014) 46–48. doi:10.1016/j.ssi.2014.05.008.
URL https://doi.org/10.1016/j.ssi.2014.05.008

[64] T. Mayeshiba, D. Morgan, Strain effects on oxygen migration in perovskites, Physical Chemistry Chemical Physics 17 (4) (2015) 2715–2721. doi:10.1039/c4cp05554c.
URL https://doi.org/10.1039/c4cp05554c